Multiple Quantum ^{13}C NMR Spectroscopy in Solids under High-Speed Magic-Angle Spinning†

Nathan A. Oyler and Robert Tycko*

Laboratory of Chemical Physics, National Institute of Diabetes and Digestive and Kidney Diseases, National Institutes of Health, Bethesda, Maryland 20892-0520

Received: April 4, 2002

We demonstrate an approach to efficient excitation and detection of high-order multiple quantum (MQ) ^{13}C NMR signals in solids under high-speed magic angle spinning (MAS). This approach combines homonuclear dipolar recoupling by the finite-pulse radio-frequency-driven recoupling (fpRFDR) pulse sequence with multiple quantum excitation pulse sequences developed for static solids based on time reversal. MQ ^{13}C NMR spectroscopy is demonstrated on the model compounds *1-^{13}C*-L-alanine, *$^{13}C_\epsilon$*-L-methionine, and *U-^{13}C,^{15}N*-L-valine, at an MAS frequency of 20.0 kHz. MQ signals resulting from coherences of 8−10 spins are observed experimentally in the singly labeled model compounds. The fpRFDR-based MQ NMR technique is also applied to both singly labeled and multiply labeled peptides in the form of amyloid fibrils. Additionally, the competition between the dipolar recoupling mechanisms of fpRFDR and delta-pulse RFDR is explored by numerical effective Hamiltonian calculations.

I. Introduction

Multiple quantum (MQ) nuclear magnetic resonance (NMR) is a form of NMR in which signals arising from coherences between spin states that differ by more than one quantum of angular momentum are detected.[1,2] In systems of coupled spin-$^1/_2$ nuclei, MQ NMR signals must arise from coherences involving multiple spins. In solids and anisotropic mesophases, MQ NMR spectroscopy is advantageous as a means of spectral simplification[3] and as a structural tool.[4−6]

In systems of many dipole-coupled nuclear spins, observation of high-order MQ NMR signals (i.e., signals from coherences involving many quanta) is generally precluded by destructive interference among unresolved MQ transitions with random phases. In 1983, Yen and Pines[7] demonstrated that this problem could be overcome by the use of MQ excitation pulse sequences that produce an effective dipole−dipole coupling Hamiltonian which is time-reversible, in other words an effective Hamiltonian of which the overall sign can be reversed by an experimental manipulation such as a radio frequency (rf) phase shift. Pulse sequences that produce time-reversible Hamiltonians which are either 2-quantum[3] or 1-quantum[8] selective have been demonstrated. Early MQ NMR experiments in solids were carried out exclusively on homogeneously broadened systems, i.e., systems in which the dipole−dipole couplings were large compared with chemical shift differences and chemical shift anisotropies (CSA). More recently, we have adapted the MQ NMR techniques based on time reversal to studies of ^{13}C-labeled organic and biochemical systems with inhomogeneously broadened spectra, i.e., systems in which the CSA exceeds the dipole−dipole couplings.[9] We have demonstrated the utility of MQ ^{13}C NMR spectroscopy as a structural probe of biological macromolecular assemblies, specifically in investigations of the structural organization of β-sheets in amyloid fibrils associated with Alzheimer's disease.[6,10]

With few exceptions, MQ NMR measurements in solids have been carried out under static sample conditions, i.e., without magic angle spinning (MAS). Although important information about the structural, dynamical, and electronic properties of certain materials can be obtained from ^{13}C NMR measurements without MAS, as demonstrated in the case of alkali fullerides by Tully and co-workers,[11] most ^{13}C NMR measurements on organic and biochemical solids are currently carried out with MAS because of the very significant enhancements in spectral resolution and sensitivity that MAS produces. Techniques for MQ proton NMR spectroscopy of solids under MAS have been demonstrated by Meier and Earl,[12] Spiess and co-workers,[13−17] and Ding and McDowell,[18] but these techniques are not effective in MQ ^{13}C NMR. Levitt and co-workers[19,20] have reported MQ ^{13}C NMR spectra of solids under MAS, but only signals up to 3-quantum were observed.

The principal difficulty with MQ ^{13}C NMR of solids under MAS is the need to generate a time-reversible effective $^{13}C-^{13}C$ dipole−dipole coupling in the presence of large chemical shift differences and CSA. Although many rf pulse sequences[21−27] for restoring the $^{13}C-^{13}C$ couplings that would otherwise be averaged out by MAS have been developed (i.e., so-called "dipolar recoupling" sequences) and some of these can produce effective dipole−dipole coupling Hamiltonians that are time-reversible under ideal conditions,[24−26] in practice the time reversibility is destroyed under more realistic or desirable conditions. In this paper, we demonstrate an approach that partly overcomes this difficulty. Our approach takes advantage of the finite-pulse radio-frequency-driven recoupling (fpRFDR) effect recently elucidated by Ishii and co-workers.[28,29] Under high-speed MAS, the fpRFDR sequence creates an effective dipole−dipole coupling Hamiltonian with the same operator form as a static coupling, even in the presence of substantial chemical shift differences and CSA. The fpRFDR sequence can then be incorporated into MQ NMR techniques developed for static

† Part of the special issue "John C. Tully Festschrift".

* To whom correspondence should be addressed. National Institutes of Health, Building 5, Room 112, Bethesda, MD 20892-0520. Phone: 301-402-8272. Fax: 301-496-0825. E-mail: tycko@helix.nih.gov.

10.1021/jp020906m CCC: $22.00
Published on Web 07/16/2002

solids,[5,8,3,7,30−32] yielding pulse sequences that we refer to as high-speed magic-angle spinning multiple quantum (HSMAS-MQ) excitation sequences. In the following sections, we demonstrate the effectiveness HSMAS-MQ sequences for MQ ^{13}C NMR both through numerical simulations and through experimental spectra of singly and multiply labeled model compounds and human Alzheimer's β-amyloid peptides in the form of amyloid fibrils. The experiments are carried out at MAS frequencies ~20.0 kHz and a magnetic field strength of 9.4 T, realistic conditions for solid-state NMR studies of many organic and biochemical systems. The experimental spectra illustrate the enhancements in sensitivity and spectral resolution (and therefore information content) that result from the ability to perform MQ ^{13}C NMR spectroscopy with high-speed MAS.

II. Theory and Simulations

General Considerations. Figure 1a illustrates the general form of a phase-incremented MQ pulse sequence.[32] The technique consists of preparation of an initial state, evolution under a MQ preparation pulse sequence (P), evolution under a MQ mixing pulse sequence (M), and signal detection. A MQ spectrum is obtained by incrementing the phase ϕ of the initial state and the P excitation sequence in a two-dimensional (2D) fashion, with $\phi = 0, 2\pi/m, ..., (m-1)2\pi/m$. The technique is performed starting with and detecting either longitudinal (I_z) or transverse (I_x) magnetization. The signal $S(\phi,0)$ at the start of detection for any crystallite may be written as

$$S(\phi,0) = \mathrm{Tr}\{I_{x,z}\mathbf{U}_\mathrm{M}\mathbf{U}_\mathrm{P}(\phi)\rho(\phi,0)\mathbf{U}_\mathrm{P}^{-1}(\phi)\mathbf{U}_\mathrm{M}^{-1}\} \quad (1a)$$

$$= \mathrm{Tr}\{[\mathbf{U}_\mathrm{M}^{-1}I_{x,z}\mathbf{U}_\mathrm{M}][R_z(\phi)\mathbf{U}_\mathrm{P}(0)I_{x,z}\mathbf{U}_\mathrm{P}(0)^{-1}R_z(-\phi)]\} \quad (1b)$$

$$= \mathrm{Tr}\{(\Sigma_{q,n}b_{q,n}A_{q,n})\,(\Sigma_{q',n'}a_{q',n'}A_{q',n'}e^{-i\,n'\,\phi})\} \quad (1c)$$

$$= \Sigma_{q,n}b^*_{q,n}a_{q,n}e^{-i\,n\,\phi} \quad (1d)$$

$$= \Sigma_{q,n}\mathrm{Re}\{b^*_{q,n}a_{q,n}\}\cos(n\phi) + Im\{b^*_{q,n}a_{q,n}\}\sin(n\phi) \quad (1e)$$

making use of the fact that the spin density operator may be decomposed at any time into a linear combination of *n*-quantum coherences, i.e., $\rho = \Sigma_{q,n}a_{q,n}A_{q,n}$ where the index q represents the different *n*-quantum operators for a multispin system.[33] The $\{A_{q,n}\}$ are *n*-quantum operators that satisfy $\mathrm{Tr}\{A^\dagger_{q,n}A_{q',n'}\} = \delta_{n,n'}\delta_{q,q'}$, $A^\dagger_{q,n} = A_{q,-n}$, and $R_z(\phi)A_{q,n}R_z(-\phi) = A_{q,n}e^{-in\phi}$. Additionally, because $\mathbf{U}I_{x,z}\mathbf{U}^{-1}$ is Hermitian, $a^*_{q,n} = a_{q,-n}$. $R_z(\phi)$ is the operator describing a rotation about z by ϕ, and $\rho(\phi,0)$ is the initial spin density operator at the beginning of the excitation pulse sequence P. In the last step, the imaginary part is identically zero after the sum over n since $a^*_{q,n} = a_{q,-n}$.

A complex Fourier transform $F(n,0)$ of $S(\phi,0)$ with respect to ϕ contains the maximum amount of information that can be known about the system. For each MQ order n, $\mathrm{Re}\{F(n,0)\} = \Sigma_q\mathrm{Re}\{b^*_{q,n}a_{q,n}\}$ and $Im\{F(n,0)\} = \Sigma_q Im\{b^*_{q,n}a_{q,n}\}$, hereafter called a MQ spectrum, represents the probability amplitude for exciting and detecting each set of *n*-quantum coherences, with the realization that destructive interference between the various q *n*-quantum coherences may have occurred. In the absence of zero filling in the ϕ dimension, Fourier transformation results in "stick" spectra in both the real and imaginary parts.

Observation of high-order multiple quantum signals is most successful when a time-reversible MQ excitation sequence (i.e., $\mathbf{U}_\mathrm{M} = \mathbf{U}_\mathrm{P}^{-1}$) is used[3,5,7,8,32−34] because the destructive interferences among the *n*-quantum coherences for different q are eliminated. In the limit of perfect time reversibility, $b_{q,n} = a_{q,n}$ and $S(\phi,0) = \Sigma_{q,n}|a_{q,n}|^2\cos(n\phi)$, for which the cosine transform is maximal and the sine transform is zero. For imperfect time reversal, the cosine transform amplitudes will be reduced and the sine transform amplitudes may be nonzero.

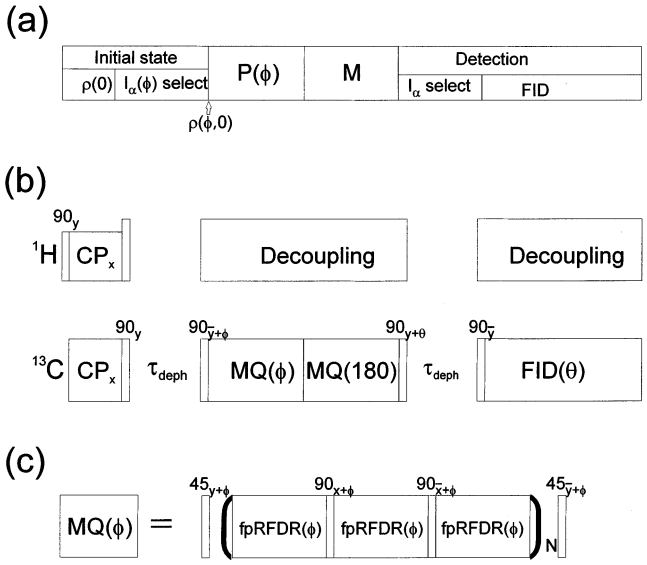

Figure 1. (a) Conceptual description of a phase-incremented multiple quantum (MQ) NMR experiment. Preparation of an initial state $\rho(\phi,0)$ (proportional to either I_z or $I_x \cos\phi + I_y \sin\phi$) is followed by preparation of MQ coherences during P, reconversion to observable magnetization during M, and detection of a selected magnetization component (proportional to either I_z or I_x). The phase ϕ is incremented in a second dimension as described in the text. (b) Experimental implementation of the double-resonance pulse sequence for MQ ^{13}C solid-state NMR with preparation and detection of transverse magnetization ($\rho(\phi,0) \propto I_x \cos\phi + I_y \sin\phi$ while detecting I_x). θ alternates between 0° and 180° to remove T_1 relaxation effects during the I_α selection block as described in the text. (c) High-speed magic-angle spinning multiple quantum (HSMAS-MQ) excitation sequence resulting from the incorporation of finite-pulse radio-frequency-driven recoupling (fpRFDR) blocks into the short two-spin, 1-quantum MQ excitation sequence designed by Suter et al.[8] for MQ NMR measurements on nonspinning solids. This excitation sequence is called "sequence A" in the text. "Sequence B" is based on the longer MQ excitation sequence of Suter et al., with eight ^{13}C $\pi/2$ pulses in the pulse cycle.

Time reversal is usually achieved by the use of excitation sequences for which the sign of the effective Hamiltonian can be reversed by an overall rf phase shift, in which case P and M are identical aside from this phase shift. Other time-reversal methods can be used, however. For example, Michal and Tycko[35] recently demonstrated high-order MQ excitation in a static solid using a single weak rf pulse for P and a sequence of hard pulses designed to reverse the spin evolution under a weak pulse for M.

The expression for $S(\phi,0)$ given above is relevant when all spins in a coupled system have equal initial polarizations and unresolved NMR frequencies in the signal detection period. If the spins have resolved NMR frequencies in the detection period but have equal initial polarizations, the detected operator $I_{x,z} = \Sigma_i I^i_{x,z}$ in eq 1a is replaced by the individual spin angular momentum operators $I^i_{x,z}$, while the initial density operator $\rho(\phi,0)$ is unchanged. Then, even in the limit of perfect time reversal, $b_{q,n} \neq a_{q,n}$ and the imaginary part of the MQ spectrum is nonzero. However, the imaginary part of the MQ spectrum must sum to zero in the case of perfect time reversal, because of the result derived above.

Finite-Pulse RFDR-Based MQ NMR Excitation. Time-reversible MQ excitation sequences with effective Hamiltonians that are two-spin, 1-quantum operators[8] and two-spin, 2-quantum operators,[7,3] have been developed for static solids. In an infinite system of dipole-coupled spin-$^1/_2$ nuclei, a two-spin, 1-quantum Hamiltonian permits the excitation of all orders of multiple quantum coherences, while a two-spin, 2-quantum Hamiltonian permits the excitation of either all odd orders or all even orders, depending on whether transverse or longitudinal spin magnetization is prepared initially and detected. In a system of N spins, the observable multiple quantum orders are further limited by selection rules.[5,8,33] When transverse magnetization is prepared initially and detected, all orders from 0 through N are observable in principle under a two-spin, 1-quantum MQ excitation Hamiltonian.

The shortest version of the two-spin, 1-quantum excitation sequence developed by Suter et al.[8] is $45_y-(-\tau/2-90_x-\tau'-90_x-\tau/2-)_n-45_{-y}$, hereafter referred to as sequence A (this sequence combined with fpRFDR is shown in Figure 1c). When the only important internal spin interactions are homonuclear dipole−dipole couplings, this sequence is sufficient to create an average dipole−dipole coupling Hamiltonian of the form $H_D^{(0)} = \sum_{i>j} d_{ij}(I_{zi}I_{xj} + I_{xi}I_{zj})$. A 180° rf phase shift (producing a rotation of the average Hamiltonian by 180° about the z component of total spin angular momentum) changes the sign of $H_D^{(0)}$. A longer version (sequence B) often used in experiments on static solids is $45_y-(-\tau/2-90_x-\tau'-90_x-\tau-90_x-\tau'-90_x-\tau-90_{-x}-\tau'-90_{-x}-\tau-90_{-x}-\tau'-90_{-x}-\tau/2-)_n-45_{-y}$. Sequence B is simply a supercycle of the shorter sequence A that additionally averages resonance offsets and chemical shifts to zero. The total MQ excitation time (τ_{MQ}) is a multiple of the cycle time of either sequence A or B. In static solids, during τ and τ' ($\tau = 2\tau' + \tau_{90}$, where τ_{90} is the length of the $\pi/2$ pulse) the system evolves under the static internal Hamiltonian of which the dipole−dipole component is proportional to the spherical tensor operator $T_{2,0}$.

Recently, Ishii[28,29] pointed out that a simple rf pulse sequence could be used under high-speed MAS to create an average Hamiltonian for a dipole-coupled spin system that is also proportional to $T_{2,0}$. This sequence consists of a single π pulse (or composite π pulse) in the middle of each rotation period, with rf phases following the XY4 pattern (or higher XY pattern).[36] The pulse sequence is identical in form to the radio-frequency-driven recoupling (RFDR) sequence introduced by Gullion and Vega[23] and by Bennett et al.,[21,27] but is executed in the regime where the π pulse lengths τ_p are a significant fraction of the MAS rotation period τ_R and where the MAS frequency ν_R is larger than chemical shift differences and CSA. In this regime, the pulse sequence is called finite-pulse RFDR (fpRFDR).

Because the average Hamiltonian under fpRFDR has the same operator form (but different spatial orientation dependence) as the homonuclear dipole−dipole coupling for a static sample, a time-reversible sequence compatible with high-speed MAS can be created by replacing τ and τ' in the excitation sequences described above by $2M$ and M rotor periods of fpRFDR respectively ($M = 8$ in the experiments below). It is immediately obvious that τ and τ' may no longer be continuous variables at any particular spinning speed, but this constraint does not significantly limit the technique's usefulness. Because fpRFDR already averages chemical shifts and CSA to zero, the shortest version of the excitation sequence (sequence A) is sufficient. We refer to fpRFDR-based MQ excitation sequences that are compatible with high-speed MAS as HSMAS-MQ excitation sequences.

Effective Hamiltonians under RFDR and fpRFDR. If the effective Hamiltonian of the fpRFDR sequence deviates from $T_{2,0}$, the HSMAS-MQ excitation sequence will not be time-reversible by a phase shift. In the limit of finite pulses with no chemical shift differences, the average Hamiltonian is proportional to $T_{2,0}$ as described by Ishii.[28] On the other hand, in the limit of delta pulses with significant chemical shift differences, the average Hamiltonian for RFDR is the "flip-flop" Hamiltonian reported by Bennett et al.,[27] which is proportional to $T_{2,0} + \sqrt{2}T_{0,0}$. Frequently, neither limit is achieved experimentally, so that a combination of the two Hamiltonians is involved. The exact experimental conditions determine the relative contributions of the two recoupling mechanisms.

To investigate the interplay between the different contributions to the effective Hamiltonian under an RFDR-type sequence, a series of simulations were performed wherein an effective coupling Hamiltonian H_{eff} was calculated for the sequence and decomposed into irreducible tensor operator components $T_{l,m}$. H_{eff} was obtained by calculating a numerically exact spin propagator, taking its logarithm, and multiplying by i/τ, where τ is the total pulse sequence time. H_{eff} was calculated in the MatLab[37] computing environment for a two spin system with isotropic chemical shifts and a dipolar coupling constant of 200 Hz. The spinning speed, chemical shift difference, and π pulse lengths were varied as described below. The propagator was calculated for each crystallite orientation by (i) dividing a single rotor period into 100 increments, (ii) calculating a "minipropagator" for each increment (including an x-phase RF field where appropriate for a total flip angle of π), (iii) multiplying the minipropagators together in a time-ordered fashion to obtain the propagator for one rotor period, (iv) rotating the resulting propagator by $e^{(-i\pi/2)I_z}$ to obtain a similar propagator for a y phase π pulse, and finally (v) multiplying the x and y phase single rotor period propagators in a time-ordered fashion to obtain a single RFDR propagator that incorporates XY8[36] phase cycling. For delta-pulse simulations, an x-phase delta pulse was inserted in the middle of a rotor period of free precession, and the full XY8 propagator was calculated in the manner described above. The logarithm of the propagator was evaluated with the MatLab function *logm*(). The coefficients $A_{l,m}$ of the $T_{l,m}$ components in H_{eff} were evaluated through the expression $A_{l,m} = \mathrm{Tr}\{T_{l,m}^\dagger H_{eff}\}/\mathrm{Tr}\{T_{l,m}^\dagger T_{l,m}\}$.

A measure of the magnitude of the delta-pulse RFDR recoupling effect is $\langle A_{0,0}^{eff}\rangle_{rms}$, which represents the root-mean-squared coefficient of $T_{0,0}$ for 500 randomly oriented crystallites. $\langle A_{2,0}^{eff}\rangle_{rms}$ has contributions from both the fpRFDR and delta-pulse RFDR recoupling mechanisms. Figure 2 shows $\langle A_{0,0}^{eff}\rangle_{rms}$ and $\langle A_{2,0}^{eff}\rangle_{rms}$ as a function of the difference in isotropic shifts for the two spins, for several values of τ_p/τ_r and two MAS speeds. As expected, in the delta-pulse limit (Figure 2a), no recoupling is observed when the chemical shift difference is zero. As the shift difference increases, the effective Hamiltonian assumes a flip-flop form, and both $\langle A_{0,0}^{eff}\rangle_{rms}$ and $\langle A_{2,0}^{eff}\rangle_{rms}$ become nonzero. The magnitude of the recoupling effect is maximal near the rotational resonance conditions ($\delta CS \sim m\nu_R$).[27] As τ_p/τ_R increases, the value of $\langle A_{2,0}^{eff}\rangle_{rms}$ at $\delta CS = 0$ increases while $\langle A_{0,0}^{eff}\rangle_{rms}$ remains equal to zero. This is the fpRFDR contribution. One expects the effective Hamiltonian to be time-reversible as long as the fpRFDR contribution dominates. From the simulations in Figure 2, time reversibility is degraded for $\delta CS > 0.3\nu_R$. This result is supported by the simulated and experimental HSMAS-MQ spectra described below.

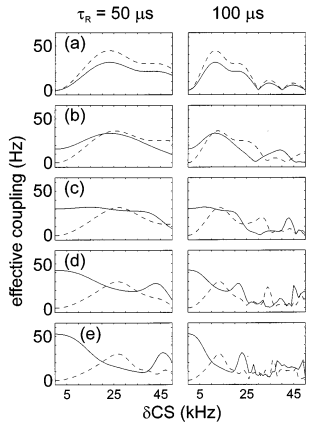

Figure 2. Effective dipole−dipole coupling Hamiltonian components $\langle A_{0,0}^{\text{eff}}\rangle_{\text{rms}}$ (dashed line) and $\langle A_{2,0}^{\text{eff}}\rangle_{\text{rms}}$ (solid line) as a function of the isotropic chemical shift difference δCS under a radio-frequency-driven recoupling (RFDR) pulse sequence, where $\langle A_{l,m}^{\text{eff}}\rangle_{\text{rms}}$ represents the root-mean-squared coefficient of the irreducible tensor operator $T_{l,m}$ in the effective Hamiltonian for 500 randomly oriented crystallites, numerically calculated for a two-spin system as described in the text. Simulations are shown for two values of the MAS rotation period τ_R and for τ_p/τ_R equal to 0.0, 0.1, 0.2, 0.3, and 0.4 (parts a−e), where τ_p is the RFDR π pulse length. The dependence of the dipolar scaling factor for finite-pulse RFDR (fpRFDR) on τ_p/τ_R is given by the magnitude of $\langle A_{2,0}^{\text{eff}}\rangle_{\text{rms}}$ at δCS = 0. Part a represents a pure "flip flop" Hamiltonian with operator form $-(\sqrt{8/3})(T_{2,0} + \sqrt{2}T_{0,0})$. In general, the coefficient of the "flip-flop" term is given by $-\sqrt{3/4}\langle A_{0,0}^{\text{eff}}\rangle_{\text{rms}}$.

Simulations of HSMAS-MQ NMR Spectra. Simulations of HSMAS-MQ NMR spectra were performed using home-built C/C++ code that calculates the full spin density matrix evolution during the simulated experiment. The internal Hamiltonian is approximated as piecewise-constant with 40−60 increments in a single rotor period. All pulses in the MQ excitation and mixing sequences are treated as finite pulses. The code is general to N spins and is capable of performing the pseudo-2D experiment, where the t_1 dimension is the phase shift ϕ, that is required for a phase-incremented MQ NMR[32] technique. Only the first signal point in t_2 is calculated to save time. Simulations for up to seven spins can be carried out before processing time becames prohibitively long. The simulated data are Fourier transformed in an identical fashion to the experimental data. The simulations included only the ^{13}C spins in all cases.

Figure 3 shows simulated MQ NMR spectra for polycrystalline *1-^{13}C*-L-alanine and $^{13}C_\epsilon$-L-methionine, containing carbonyl and methyl ^{13}C labels, respectively. The simulations are based on the crystal structures for alanine[38] with one crystallographically inequivalent molecule and methionine[39] with two inequivalent molecules. The minimum distance between labeled sites in *1-^{13}C*-L-alanine is 4.16 Å.[38] In $^{13}C_\epsilon$-L-methionine, the minimum distance is 3.77 Å.[39] Seven labeled sites are included in the simulations, contained within a sphere with radius ∼5 Å. Only signals of the central atom are detected, to minimize edge effects. The CSA tensor values were measured on the two samples and included in the simulations. The CSA tensor orientation for the alanine carbonyl (anisotropy ∼130 ppm) is based on values measured previously by Naito et al.[40] The methionine methyl CSA (anisotropy ∼15 ppm) orientation is assumed to have its largest component along the methyl rotor axis. The simulations assumed a 9.4 T magnetic field, a spinning frequency of 20 kHz, a 20 μs π pulse for the fpRFDR sequence, and a 4 μs $\pi/2$ pulse. The simulations used excitation sequence B with $M = 16$, yielding a cycle time of 9.6 ms. The simulated buildup of MQ signal amplitudes is similar for the two

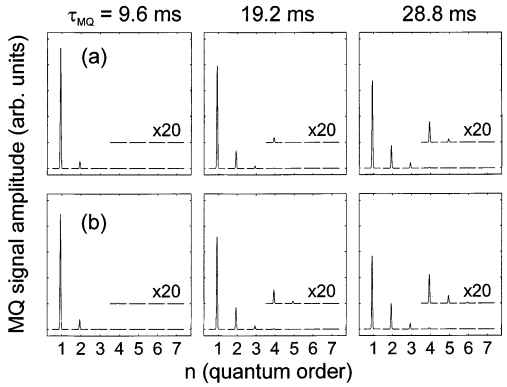

Figure 3. (a) Simulated HSMAS-MQ NMR spectra for a seven-spin system representing *1-^{13}C*-L-alanine for the indicated values of the MQ excitation time. (b) Simulated HSMAS-MQ spectra for a seven-spin system representing $^{13}C_\epsilon$-L-methionine, observing one of the two crystallographically inequivalent sites. Line shapes are Gaussians, multiplied by the simulated MQ signal amplitudes. Simulation conditions: $\nu_R = 20.0$ kHz, sequence B (described in the text) with $M = 16$ and XY16 phase cycling, fpRFDR π pulse = 20 μs, $\pi/2$ pulse = 4 μs.

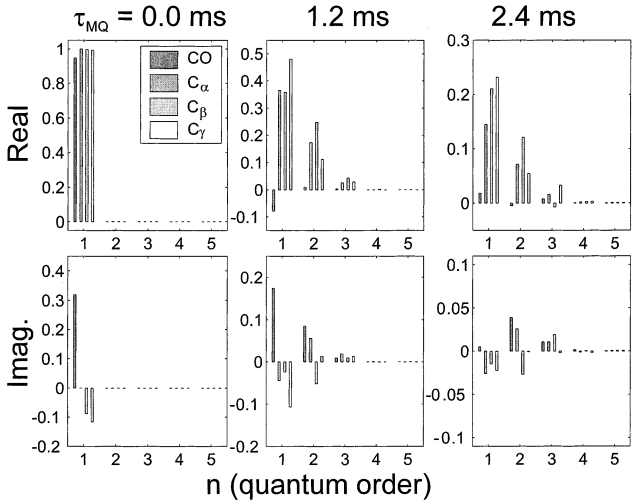

Figure 4. Simulations of the real and imaginary parts of the HSMAS-MQ signal amplitudes for a five-spin system, similar to the five ^{13}C sites in L-valine, including all terms in the internal Hamiltonian (dipolar interactions, CSA, chemical shift differences and J couplings) for the indicated MQ excitation times. The simulated signals detected at the carbonyl, C_α, C_β, and the two C_γ carbons are presented as bar plots. Simulation conditions: $\nu_R = 20.0$ kHz, sequence A (described in the text) with $M = 8$ and XY8 phase cycling, fpRFDR π pulse = 20 μs, $\pi/2$ pulse = 5 μs.

compounds, despite the large difference in CSA. The total signal intensity for $^{13}C_\epsilon$-L-methionine is slightly reduced compared to *1-^{13}C*-L-alanine due to the effect of the 1.5 ppm chemical shift difference between the two resolved crystallographic sites. Simulations for $^{13}C_\epsilon$-L-methionine without the chemical shift difference were nearly identical to those for *1-^{13}C*-L-alanine, indicating that the HSMAS-MQ excitation sequence is insensitive to the CSA.

Simulations for *U-^{13}C,^{15}N*-L-valine are shown in Figures 4 and 5, based on one of the two inequivalent molecules in its crystal structure.[39] The CSA tensor values of the carbonyl carbon were measured by slow-spinning ^{13}C MAS NMR experiments on unlabeled polycrystalline L-valine, and its orientation is assumed to be similar to that for L-alanine.[40] The other carbons in valine have small anisotropies for which accurate determination of the CSA asymmetry (η) values is difficult. From visual inspection of slow-spinning ^{13}C MAS NMR spectra, the η values all appear close to one. The simulations assume that the α, β,

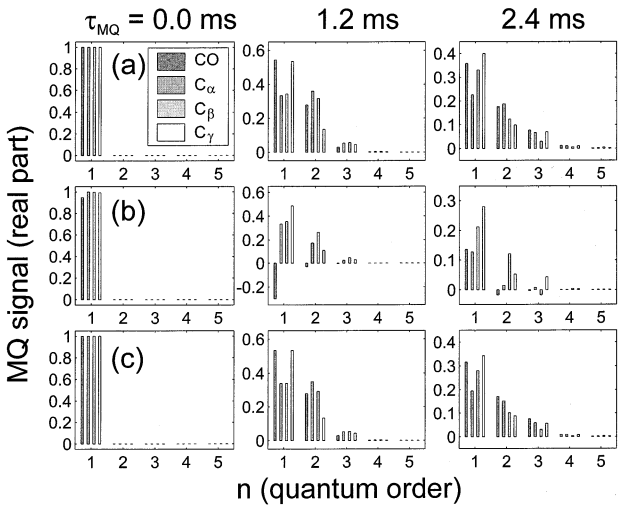

Figure 5. Simulations of the real part of the HSMAS-MQ signal amplitudes for a five-spin system, as in Figure 4, but including only selected terms of the internal Hamiltonian. (a) Dipole−dipole couplings only. (b) Dipole−dipole couplings and chemical shift differences only. (c) Dipole−dipole couplings and *J* couplings only. Simulation conditions were identical to those in Figure 4.

and γ carbons have $\eta = 1$ CSA tensors with measured anisotropies and estimated orientations. Isotropic chemical shift differences were measured from MAS spectra. The *J* couplings were assumed to be the following: $CO-C_\alpha = 50$ Hz, $C_\alpha-C_\beta = 40$ Hz, and $C_\beta-C_\gamma = 30$ Hz. The carrier frequency is the same as the C_α frequency in the simulations shown in Figures 4 and 5, which also assume a 9.4 T magnetic field, a spinning frequency of 20 kHz, a 20 μs π pulse for the fpRFDR sequence, and a 5 μs π pulse. The MQ excitation sequence shown in Figure 1c (sequence A) was used in these simulations, with $M = 8$, giving a 1.2 ms cycle time.

Figure 4 shows the real and imaginary parts of the HSMAS-MQ signals from simulations including all terms of the internal Hamiltonian (dipole−dipole couplings, CSA, chemical shift differences, and *J* couplings). Because the $^{13}C-^{13}C$ dipole−dipole couplings between directly bonded carbons are large (∼2 kHz), the spin system is nearly fully excited after only 1.2 ms of MQ excitation. Significant 1-, 2-, and 3-quantum signals are observed. Amplitudes of 4- and 5-quantum signals are small, presumably due to the relatively small number of possible 4- and 5-quantum transitions. In a uniformly labeled molecule such as *U-*^{13}*C,*^{15}*N*-L-valine, isotropic shift differences and *J* couplings both interfere with the time-reversibility of the MQ excitation sequence. The effects of isotropic shift differences and *J* couplings are explored in Figure 5, which shows the real parts of simulations with only the dipole−dipole couplings (Figure 5a), the dipole−dipole couplings and chemical shift differences (Figure 5b), and the dipole−dipole couplings and *J* couplings (Figure 5c). Both the chemical shift differences and the *J* couplings dampen the MQ signal amplitudes noticeably. In the case of the shift differences, this is because the shift differences are not very small compared with the MAS frequency, resulting in an effective Hamiltonian that deviates significantly from the ideal fpRFDR average Hamiltonian. The *J* couplings are not averaged to zero by the fpRFDR sequence and are not time-reversed by a phase shift of either sequence A or sequence B.

III. Experimental Methods

Sample Preparation. Polycrystalline *1-*^{13}*C*-L-alanine and *U-*^{13}*C,*^{15}*N*-L-valine were purchased from Cambridge Isotopes Laboratories. Polycrystalline *$^{13}C_\epsilon$*-L-methionine was purchase from Sigma Chemical Co. The 40-residue human β-amyloid peptide associated with Alzheimer's disease ($A\beta_{1-40}$) was synthesized, purified, fibrillized by incubation of a 1 mM aqueous solution at pH 7.4, and lyophilized as previously described.[6] A *1-*^{13}*C*-L-valine residue was incorporated synthetically at position 39 in the amino acid sequence (Val39). Unfibrillized $A\beta_{1-40}$ was purified and lyophilized without incubation. The seven-residue peptide $A\beta_{16-22}$, comprising residues 16−22 of $A\beta_{1-40}$ with amide- and acetyl-capping groups at the N- and C-termini, was prepared and fibrillized as described.[28,10] The $A\beta_{16-22}$ peptide was uniformly ^{15}N- and ^{13}C-labeled at five successive residues, namely Leu17, Val18, Phe19, Phe20, and Ala21.

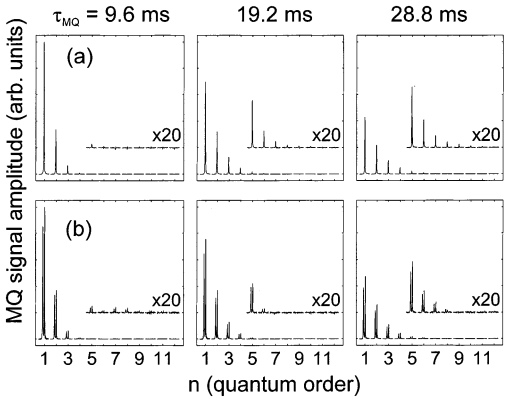

Figure 6. (a) Real part of the experimental HSMAS-MQ spectra for *1-*^{13}*C*-L-alanine corresponding to 9.6, 19.2 and 28.8 ms MQ excitation times, obtained at 100.4 MHz ^{13}C NMR frequency with 64 increments in ϕ and 120 scans per ϕ value. (b) Real part of the experimental HSMAS-MQ spectra for *$^{13}C_\epsilon$*-L-methionine, obtained at 100.4 MHz ^{13}C NMR frequency with 64 increments in ϕ and 96 scans per ϕ value. Each sample (approximately 8 mg) was restricted to the center 60% of the MAS rotor to minimize rf inhomogeneity effects. Each experiment required 5−6 h of spectrometer time. Experimental conditions: $\nu_R = 20.0$ kHz, sequence B (described in the text) with $M = 8$ and XY8 phase cycling, fpRFDR π pulse = 20 μs, $\pi/2$ pulse = 3 μs.

NMR Spectroscopy. Figure 1 presents the various details of the HSMAS-MQ ^{13}C NMR technique. Figure 1a is the conceptual depiction of the sequence described earlier. The I_α selection sequences are required to ensure that only one component of the magnetization is observed or prepared. The I_α selection sequence ($90_y-\tau_{deph}-90_{-y}$) relies on T_2 relaxation processes, which act faster without proton decoupling, to dephase the transverse components of the magnetization during τ_{deph}. Phase alternation of the $\pi/2$ pulse at the end of the MQ mixing period and alternate addition and subtraction of FID signals were employed to cancel out signal contributions from magnetization that develops during τ_{deph} through T_1 relaxation. In the case of uniformly labeled samples (Figures 8 and 9), $^{13}C-^{13}C$ spin diffusion during τ_{deph} can redistribute spin polarization among the inequivalent carbon sites, distorting the MQ signal amplitudes. For these samples, τ_{deph} was set to zero.

Figure 1b depicts the experimental implementation of the phase-incremented technique in which transverse magnetization is prepared and detected. Cross polarization is used to generate an initial ^{13}C magnetization along the *x* axis, followed by flip-up pulse of fixed phase y. After dephasing of any residual transverse magnetization, a flip-down pulse of phase $-y + \phi$ provides transverse magnetization with phase ϕ. The two-spin, 1-quantum excitation sequence incorporating fpRFDR is applied with the overall phase shift ϕ, followed by the same sequence applied with a fixed 180° phase shift for time reversal. Finally,

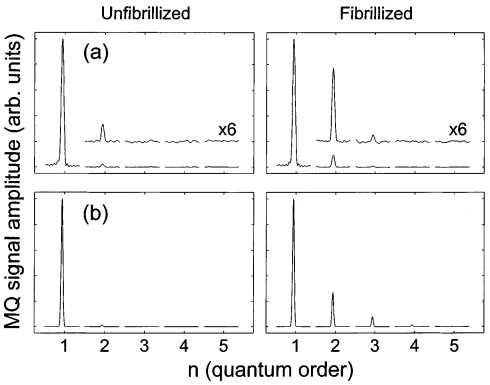

Figure 7. (a) Real parts of the experimental HSMAS-MQ spectra of the human Alzheimer's β-amyloid peptide Aβ_{1-40} with a single ^{13}C label at the carbonyl site of Val39, obtained at 100.4 MHz ^{13}C NMR frequency with $\tau_{MQ} = 31.1$. Spectra of unfibrillized Aβ_{1-40} (left) and amyloid fibrils (right) are shown, each with 32 increments in ϕ and 1600 scans per ϕ value (approximately 28 h, approximately 8 mg samples). Experimental conditions: $\nu_R = 18.519$ kHz, sequence B (described in the text) with $M = 8$ and XY8 phase cycling, fpRFDR π pulse = 20 μs, $\pi/2$ pulse = 4 μs. (b) Simulated spectra for isolated ^{13}C labels with couplings to natural abundance ^{13}C spins only (left) and for 6 carbonyl ^{13}C labels spaced linearly 4.8 Å apart. Line shapes are Gaussians, multiplied by the simulated MQ signal amplitudes.

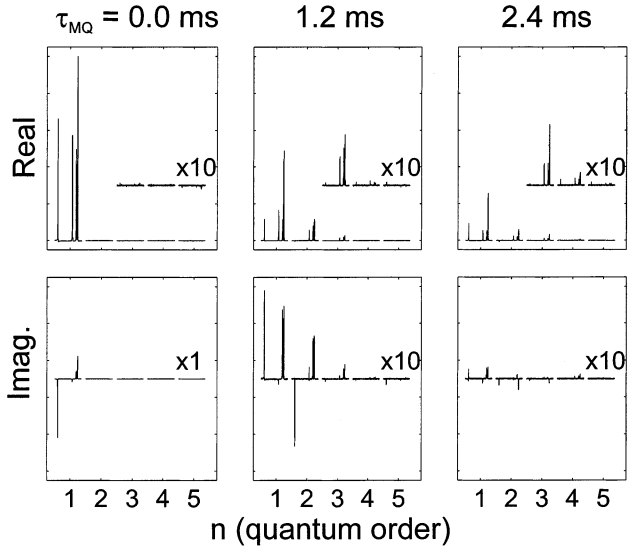

Figure 8. Real and imaginary parts of the experimental HSMAS-MQ spectra of polycrystalline *U-^{13}C,^{15}N*-L-valine for the indicated MQ excitation times, 16 increments in ϕ, and 200 scans per ϕ value. Approximately 8 mg sample restricted to the center of the MAS rotor. Experimental conditions: $\nu_R = 20.000$ kHz, sequence A (described in the text) with $M = 8$ and XY8 phase cycling, fpRFDR π pulse = 20 μs, $\pi/2$ pulse = 3.7 μs.

the *x* component of the magnetization was selected for detection as described above. Sequence A was used for uniformly labeled samples (Figure 1c.). Sequence B was used in the experiments on singly labeled samples. The fpRFDR blocks consist of $M =$ 8 or 16 rotor periods of fpRFDR subjected to XY8 or XY16 phase cycling.

Experiments were performed on a Varian/Chemagnetics Infinity NMR spectrometer operating at a proton frequency of 399.2 MHz, using a Varian/Chemagnetics 3.2 mm MAS NMR probe. Cross polarization was achieved by applying a 70 kHz rf field on protons and linearly ramping the ^{13}C rf field over a 30% range centered at 50 kHz. Proton decoupling was maintained at 110 kHz during the MQ excitation and mixing sequences, and 75 kHz during signal detection. The fpRFDR

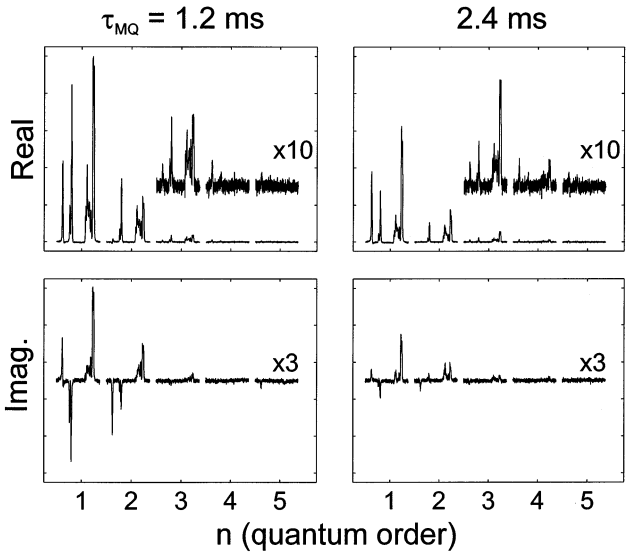

Figure 9. Real and imaginary parts of the experimental HSMAS-MQ spectra of fibrillized Aβ_{16-22} (residues 16−22 of Aβ_{1-40}, with amide and acetyl capping groups at the C- and N-termini), with uniform ^{13}C and ^{15}N labeling of Leu17, Val18, Phe19, Phe20, and A21. Obtained at a ^{13}C NMR frequency of 100.4 MHz with the indicated MQ excitation times, 16 increments in ϕ, and 512 scans per ϕ value. The 3 mg sample was restricted to the center of the rotor. Experimental conditions: $\nu_R = 20.000$ kHz, sequence A (described in the text) with $M = 8$ and XY8 phase cycling, fpRFDR π pulse = 20 μs, $\pi/2$ pulse = 3.7 μs.

180° pulse lengths were 20 μs. Spectral artifacts were minimized by CYCLOPS phase cycling of the final ^{13}C $\pi/2$ pulse. Experiments on Aβ_{1-40} samples were performed with pulsed spin-lock detection for sensitivity enhancement.[41] The phase shift ϕ varied over 360° in either 16, 32, or 64 steps. Block averaging of the 2D data sets was employed to minimize artifacts due to spectrometer instabilities.

IV. Experimental Results

Singly Labeled Compounds. Figure 6 shows experimental HSMAS-MQ ^{13}C NMR spectra of *1-^{13}C*-L-alanine and *$^{13}C_\epsilon$*-L-methionine. A 10-quantum signal is observed in *1-^{13}C*-L-alanine, and 8-quantum signals are observed in *$^{13}C_\epsilon$*-L-methionine at $\tau_{MQ} = 28.8$ ms. The extent of high-order MQ excitation is apparently similar to previously reported results for the same samples under static conditions,[9] although longer excitation times are required because of the reduction in ^{13}C−^{13}C coupling strengths due to the scaling factor of the fpRFDR sequence. Comparison with the simulated spectra in Figure 2 is only relevant to the extent that the pattern of MQ intensities is qualitatively similar since the simulations only included seven spins, while coherences involving 8−10 spins are observable experimentally. For both samples, the 7-quantum signal intensity is about 1% of that for the 1-quantum signal, making this the practical observable limit for similar intermolecular distances under less favorable circumstances (e.g., molecules with higher molecular weight). The experiments confirm the relative insensitivity of the HSMAS-MQ technique to the anisotropy of the chemical shift.

The observation of two methyl carbon signals in each MQ order for *$^{13}C_\epsilon$*-L-methionine illustrates the enhanced spectral resolution, and in principle enhanced information content, in MQ ^{13}C NMR spectra obtained under MAS conditions. In MQ NMR experiments on static *$^{13}C_\epsilon$*-L-methionine, these signals from inequivalent sites are not resolved.[9] These signals are also not resolved when pulsed spin locking is used for line narrowing

and sensitivity enhancement in MQ NMR measurements on static samples.[41]

As an application of the HSMAS-MQ technique to a system of biochemical interest, MQ ^{13}C NMR spectra of fibrillized and unfibrillized Aβ_{1-40}, ^{13}C-labeled at the carbonyl site of Val39, are presented in Figure 7a. Previous solid-state NMR data, including MQ NMR data on static samples, indicate that a central segment and the C-terminal segment of the Aβ_{1-40} peptide form parallel β-sheets in the amyloid fibrils, with an "in-register" intermolecular hydrogen bonding pattern.[6,42] The previous MQ NMR measurements on Aβ_{1-40} were carried out on static samples with labels at methyl carbon sites. Signals up to at least 4-quantum were observed at $\tau_{MQ} = 14.4$ ms, in quantitative agreement with numerical simulations for a parallel β-sheet structure with 4.8 Å spacings between peptide chains.[6] Attempts to perform quantitative MQ NMR measurements on static Aβ_{1-40} samples with carbonyl labels were unsuccessful due to inefficient MQ excitation in the presence of large CSA (unpublished data). The MQ ^{13}C NMR spectra in Figure 7a show significant 2- and 3-quantum signals in fibrillized Aβ_{1-40}, but a weaker 2-quantum signal and no detectable 3-quantum signal in unfibrillized Aβ_{1-40}. This result demonstrates the potential of HSMAS-MQ ^{13}C NMR measurements as structural probes of biochemical systems and the applicability of such measurements to samples that are labeled at sites with large CSA. For comparison with the experimental spectra, Figure 7b shows numerical simulations for a single ^{13}C label surrounded by natural-abundance carbons, as well as for six carbonyl carbons in a line with 4.8 Å spacings. These simulations show that the weak 2-quantum signal observed in experimental HSMAS-MQ spectra of the unfibrillized Aβ_{1-40} sample can be attributed to ^{13}C-^{13}C dipole−dipole couplings to natural-abundance ^{13}C spins, but that the 2- and 3-quantum signals observed in experimental spectra of the fibrillized sample arise from intermolecular couplings between labels on neighboring peptide chains in the β-sheets of the amyloid fibril structure. We attribute the absence of quantitative agreement between experiments and simulations for the fibrillized sample to effects of pulse sequence imperfections and T_2-spin-relaxation processes in the rather long (31.1 ms) MQ excitation periods.

Uniformly Labeled Compounds. Figure 8 shows experimental HSMAS-MQ ^{13}C NMR spectra of *U-^{13}C,^{15}N*-L-valine. Both the real and the imaginary parts of the spectra are shown for two values of τ_{MQ}. As predicted by the simulations in Figures 4 and 5, significant 1-, 2-, and 3-quantum signals are observed, but 4- and 5-quantum signals are small. MQ signal amplitudes are maximized at the shortest τ_{MQ} value and decrease rapidly with increasing τ_{MQ}. As discussed above in the context of the simulations, this behavior is a consequence of the large intramolecular ^{13}C-^{13}C dipole−dipole couplings and the imperfect time-reversibility of the MQ excitation sequence due to large isotropic chemical shift differences and J couplings. Quantitative differences between experimental and simulated MQ signal amplitudes are most likely due to the approximate CSA tensor values and orientations used in the simulations.

As a final experimental demonstration of HSMAS-MQ ^{13}C NMR, Figure 9 shows spectra of the Aβ_{16-22} fibril sample, containing five uniformly labeled residues. The same sample was used in earlier studies by 2D ^{13}C-^{13}C exchange spectroscopy that established a highly ordered β-strand conformation for the labeled segment in the fibrils.[10,28] The HSMAS-MQ NMR spectra show significant 1-, 2-, and 3-quantum signals, with maximal signal amplitudes at $\tau_{MQ} = 1.2$ ms. These spectra are the first MQ solid state ^{13}C NMR spectra of a biochemically significant sample with uniform ^{13}C labeling. Simulations of the dependence of the MQ signal amplitudes on molecular conformation (data not shown) indicate that the spectra in Figure 9 do not by themselves contain significant structural information, i.e., they do not depend strongly on the torsion angles that define the conformations of individual residues. However, it is likely that important structural information may be obtained from MQ ^{13}C NMR measurements that include an additional period of spin evolution under heteronuclear dipole−dipole couplings[20,43−46] or chemical shifts.[46,47−49] Such an evolution period would occur between the P and M periods in Figure 1A. The experimental results in Figure 9 set the stage for future structural measurements along these lines.

V. Discussion

The simulations and experimental results reported above demonstrate that high-order MQ ^{13}C NMR signals can be excited and detected under high-speed MAS conditions through the use of a simple rf pulse sequence based on the combination of fpRFDR recoupling with time-reversal sequences developed originally for static samples. Excitation of high-order intermolecular MQ coherences is possible with relatively long excitation periods ($\tau_{MQ} > 10$ ms) and is most successful when isotropic shift differences are small. The HSMAS-MQ sequences are relatively insensitive to chemical shift anisotropy, permitting experiments samples with labels at sites with large CSA. Experiments on uniformly labeled compounds, in which intramolecular MQ coherences are observed, require relatively short excitation periods ($\tau_{MQ} \sim 1$ ms). Imperfect time reversal due to isotropic chemical shift differences and J couplings reduces the MQ signal amplitudes at longer excitation periods. Experimental observation of signals in the highest MQ orders ($n = N - 1$ and $n = N$ in an N-spin system) is generally precluded by the inherently low excitation probability amplitude for these signals.

HSMAS-MQ measurements have the potential to provide important structural constraints on biochemical systems and other complex organic solids. Intermolecular MQ signal amplitudes provide information about supramolecular structure, as demonstrated by the experimental results in Figure 7. Excitation of intramolecular MQ coherences in uniformly labeled samples may permit measurements of the conformations of monomer units in biopolymers when additional spectroscopic dimensions are added to the HSMAS-MQ technique. The development of a simple and efficient approach to MQ excitation under high-speed MAS, as described above, opens the way for further investigations into the utility of MQ ^{13}C NMR as a structural tool.

Acknowledgment. We thank Dr. John J. Balbach for providing the Aβ_{1-40} and Dr. Y. Ishii for providing the Aβ_{16-22} samples used in this work. We thank Dr. Ani T. Petkova for suggesting the importance of J coupling effects in MQ spectra of uniformly labeled samples. This work was supported in part by the Intramural AIDS Targeted Antiviral Program of the National Institutes of Health.

References and Notes

(1) Weitekamp, D. P. *Adv. Magn. Reson.* **1983**, *11*, 111−274.

(2) Bodenhausen, G. *Prog. Nucl. Magn. Reson. Spectrosc.* **1980**, *14*, 137−173.

(3) Warren, W. S.; Weitekamp, D. P.; Pines, A. *J. Chem. Phys.* **1980**, *73*, 2084−2099.

(4) Baum, J.; Gleason, K. K.; Pines, A.; Garroway, A. N.; Reimer, J. A. *Phys. Rev. Lett.* **1986**, *56*, 1377−1380.

(5) Baum, J.; Pines, A. *J. Am. Chem. Soc.* **1986**, *108*, 7447−7454.
(6) Antzutkin, O. N.; Balbach, J. J.; Leapman, R. D.; Rizzo, N. W.; Reed, J.; Tycko, R. *Proc. Natl. Acad. Sci. U.S.A.* **2000**, *97*, 13045−13050.
(7) Yen, Y. S.; Pines, A. *J. Chem. Phys.* **1983**, *78*, 3579−3582.
(8) Suter, D.; Liu, S. B.; Baum, J.; Pines, A. *Chem. Phys.* **1987**, *114*, 103−109.
(9) Antzutkin, O. N.; Tycko, R. *J. Chem. Phys.* **1999**, *110*, 2749−2752.
(10) Balbach, J. J.; Ishii, Y.; Antzutkin, O. N.; Leapman, R. D.; Rizzo, N. W.; Dyda, F.; Reed, J.; Tycko, R. *Biochemistry* **2000**, *39*, 13748−13759.
(11) Tycko, R.; Dabbagh, G.; Rosseinsky, M. J.; Murphy, D. W.; Flemming, R. M.; Ramirez, A. P.; Tully, J. C. *Science* **1991**, *253*, 884−886.
(12) Meier, B. H.; Earl, W. L. *J. Chem. Phys.* **1986**, *85*, 4905−4911.
(13) Geen, H.; Graf, R.; Heindrichs, A. S. D.; Hickman, B. S.; Schnell, I.; Spiess, H. W.; Titman, J. J. *J. Magn. Reson.* **1999**, *138*, 167−172.
(14) Friedrich, U.; Schnell, I.; Brown, S. P.; Lupulescu, A.; Demco, D. E.; Spiess, H. W. *Mol. Phys.* **1998**, *95*, 1209−1227.
(15) Geen, H.; Titman, J. J.; Gottwald, J.; Spiess, H. W. *J. Magn. Reson., Ser. A* **1995**, *114*, 264−267.
(16) Geen, H.; Titman, J. J.; Gottwald, J.; Spiess, H. W. *Chem. Phys. Lett.* **1994**, *227*, 79−86.
(17) Gottwald, J.; Demco, D. E.; Graf, R.; Spiess, H. W. *Chem. Phys. Lett.* **1995**, *243*, 314−323.
(18) Ding, S.; McDowell, C. A. *J. Magn. Reson., Ser. A* **1996**, *120*, 261−263.
(19) Eden, M.; Levitt, M. H. *Chem. Phys. Lett.* **1998**, *293*, 173−179.
(20) Eden, M.; Brinkmann, A.; Luthman, H.; Eriksson, L.; Levitt, M. H. *J. Magn. Reson.* **2000**, *144*, 266−279.
(21) Bennett, A. E.; Ok, J. H.; Griffin, R. G.; Vega, S. *J. Chem. Phys.* **1992**, *96*, 8624−8627.
(22) Gregory, D. M.; Mitchell, D. J.; Stringer, J. A.; Kiihne, S.; Shiels, J. C.; Callahan, J.; Mehta, M. A.; Drobny, G. P. *Chem. Phys. Lett.* **1995**, *246*, 654−663.
(23) Gullion, T.; Vega, S. *Chem. Phys. Lett.* **1992**, *194*, 423−428.
(24) Lee, Y. K.; Kurur, N. D.; Helmle, N.; Johannessen, O. G.; Nielsen, N. C.; Levitt, M. H. *Chem. Phys. Lett.* **1995**, *242*, 304−309.
(25) Sun, B. Q.; Costa, P. R.; Kocisco, D.; Lansbury, P. T.; Griffin, R. G. *J. Chem. Phys.* **1992**, *102*, 702−707.
(26) Tycko, R.; Smith, S. O. *J. Chem. Phys.* **1993**, *98*, 932−943.
(27) Bennett, A. E.; Rienstra, C. M.; Griffiths, J. M.; Zhen, W.; Lansbury, P. T., Jr; Griffin, R. G. *J. Chem. Phys.* **1998**, *108*, 9463−9479.
(28) Ishii, Y. *J. Chem. Phys.* **2001**, *114*, 8473−8483.
(29) Ishii, Y.; Balbach, J. J.; Tycko, R. *Chem. Phys.* **2001**, *266*, 231−236.
(30) Baum, J.; Munowitz, M.; Garroway, A. N.; Pines, A. *J. Chem. Phys.* **1985**, *83*, 2015−2025.
(31) Munowitz, M.; Pines, A.; Mehring, M. *J. Chem. Phys.* **1987**, *86*, 3172−3182.
(32) Shykind, D. N.; Baum, J.; Liu, S. B.; Pines, A.; Garroway, A. N. *J. Magn. Reson.* **1988**, *76*, 149−154.
(33) Tycko, R. *J. Magn. Reson.* **1999**, *139*, 302−307.
(34) Baum, J.; Munowitz, M.; Garroway, A. N.; Pines, A. *J. Chem. Phys.* **1985**, *83*, 2015−2025.
(35) Michal, C. A.; Tycko, R. *J. Chem. Phys.* **2001**, *114*, 409−415.
(36) Gullion, T.; Baker, D. B.; Conradi, M. S. *J. Magn. Reson.* **1990**, *89*, 479−484.
(37) *MatLab*, version 5.3.0; Mathworks, Inc.: Natick, MA, 1999.
(38) Destro, R.; Marsh, R. E.; Bianchi, R. *J. Phys. Chem.* **1988**, *92*, 966−973.
(39) Dalhus, B.; Gorbitz, C. H. *Acta Chem. Scand.* **1996**, *50*, 544.
(40) Naito, S.; Ganapathy, S.; Akasaka, K.; McDowell, C. A. *J. Chem. Phys.* **1981**, *74*, 3190−3197.
(41) Petkova, A. T.; Tycko, R. *J. Magn. Reson.* **2002**. In press.
(42) Balbach, J. J.; Petkova, A. T.; Oyler, N. A.; Antzutkin, O. N.; Gordon, D. J.; Meredith, S. C.; Tycko, R. *Biophys. J.* **2002**. In press.
(43) Costa, P. R.; Gross, J. D.; Hong, M.; Griffin, R. G. *Chem. Phys. Lett.* **1997**, *280*, 95−103.
(44) Feng, X.; Lee, Y. K.; Sandstrom, D.; Eden, M.; Maisel, H.; Sebald, A.; Levitt, M. H. *Chem. Phys. Lett.* **1996**, *257*, 314−320.
(45) Feng, X.; Eden, M.; Brinkmann, A.; Luthman, H.; Eriksson, L.; Graslund, A.; Antzutkin, O. N.; Levitt, M. H. *J. Am. Chem. Soc.* **1997**, *119*, 12006−12007.
(46) Schmidt-Rohr, K. *J. Am. Chem. Soc.* **1996**, *118*, 7601−7603.
(47) Blanco, F. J.; Tycko, R. *J. Magn. Reson.* **2001**, *149*, 131−138.
(48) Bower, P. V.; Oyler, N. A.; Mehta, M. A.; Long, J. R.; Stayton, P. S.; Drobny, G. P. *J. Am. Chem. Soc.* **1999**, *121*, 8373−8375.
(49) Gregory, D. M.; Mehta, M. A.; Shiels, J. C.; Drobny, G. P. *J. Chem. Phys.* **1997**, *107*, 28−42.